Journal of Applied Electrochemistry (2005) 35:975–984
DOI 10.1007/s10800-005-6726-x

Passivity and corrosion of Cu–*x*Zn (*x* = 10–40 wt%) alloys in borate buffer containing chloride ions

T. KOSEC. MIKIĆ[1], I. MILOŠEV[1,2,*] and B. PIHLAR[3]
[1]*Department of Physical and Organic Chemistry, Jožef Stefan Institute, Jamova 39, 1000 Ljubljana, Slovenia*
[2]*Orthopaedic Hospital Valdoltra, Jadranska c. 31, 6280, Ankaran, Slovenia*
[3]*Faculty of Chemistry and Chemical Technology, University of Ljubljana, Aškerčeva 5, 1000, Ljubljana, Slovenia*
*(*author for correspondence, fax: +386-1-4773 811; e-mail, ingrid.milosev@ijs.si)*

Received 4 January 2005; accepted in revised form 18 April 2005

Key words: borate solution, chloride ions, Cu–*x*Zn alloy, cyclic voltammetry, pitting corrosion

Abstract

The electrochemical behaviour of Cu–*x*Zn alloys and of Cu and Zn metals was studied by cyclic voltammetry and chronopotentiometry in borate buffer, pH = 9.2, with and without the addition of chloride ions in the range from 0.01 M to 1 M. In general, the shape of voltammograms of four Cu–*x*Zn alloys with 10 – 40 wt.% of zinc resembles that of copper more than that of zinc. With increasing zinc content several characteristics of zinc are observed. In borate buffer containing chloride anions, Cu–*x*Zn alloys are susceptible to pitting corrosion. The breakdown potential, E_b, at which the current density in the passive region starts to increase abruptly, becomes more negative with increasing zinc content in the alloy. The general relationship $E_b = a + b \log c_{NaCl}$ held in all cases, with constants *a* and *b*, however, being dependent on the zinc content of the alloy and on the chloride concentration. The corrosion resistance of Cu–*x*Zn alloys was less than that of copper metal but significantly greater than that of zinc.

1. Introduction

Brasses are technologically important materials and have been studied extensively, especially in terms of dezincification [1–3], corrosion inhibition [4–9] and stress corrosion cracking [10–14]. Passivation in slightly alkaline solution, with and without addition of chloride, has not received much attention [15–20]. The passivation behaviour of brasses under these conditions is interesting since the passivation of the copper and zinc components occurs at a pH value of 9 [21]. It has been recognized that the passivation of brasses is based on the formation of a complex oxide layer consisting of ZnO and Cu_2O and CuO [16–21]. Morales et al. studied extensively α-, (α + β)- and β-brasses with Zn contents of 28 wt.%, 39 wt.% and 48 wt.%, respectively [17–19]. In the presence of chloride ions the resistance to localized corrosion decreased with increasing zinc content [17]. Localized corrosion resistance was significantly improved in the lower potential range, where zinc itself is active. Rudd and Breslin reported that UV illumination has an activating effect on the passivation of Cu–37Zn in chloride containing borate buffer [20]. Their results were explained in terms of the nature of complex films involving $ZnO{\cdot}xH_2O$ and Cu_2O/CuO oxides. On illumination, photodecomposition of the n-type ZnO layer occurs, leading to a modification of the passive film that renders it more susceptible to pitting attack in a chloride environment [21]. The issue of selective dissolution was studied in slightly acid [22] and slightly alkaline solutions [23]. The preferential dissolution of zinc occurred at negative potentials, leaving the surface enriched in copper. As the potential shifted in the more noble direction, simultaneous dissolution of both components took place [22, 23].

The behaviour of the individual metal components, Cu and Zn, has been studied extensively. The passivation of Cu is established as being due to formation of a duplex Cu_2O/CuO layer [24–26], whereas a $ZnO/Zn(OH)_2$ layer is responsible for passivation of Zn [27–29]. Various commercial brasses have been described, for example 61Cu–35Zn–3.25Pb [15], 58Cu–40Zn–1.8Pb and 58Cu–38Zn–3.5Pb [30], Cu37Zn brass [20, 22], and α-, (α + β)- and β-brasses [17–19]. In our previous work the passivation behaviour of a series of Cu–*x*Zn alloys (*x* = 10, 20, 30 and 40 wt.%) and Cu and Zn metals was studied in borate buffer, pH = 9.2, by a combination of electrochemical measurements and X-ray photoelectron spectroscopy (XPS) [16]. The passive film formed on Cu–10Zn and Cu–20Zn alloys consists of Cu_2O and CuO, together with a small amount of ZnO. The content of ZnO in the passive film increases with increasing zinc content in the alloy. In the present work the behaviour of Cu–*x*Zn alloys and individual metal components Cu and Zn is

studied in borate buffer solution with and without the addition of chloride ions, with a special emphasis on measurement of breakdown potentials as a function of chloride concentration and zinc content.

2. Experimental details

Copper–zinc alloys, Cu–*x*Zn, (Wieland-Werke AG, Ulm, Germany) are denoted according to their zinc content: Cu–10Zn, Cu–20Zn, Cu–30Zn and Cu–40Zn, where *x* is zinc content in wt.%. Copper (99.999%) and zinc samples (99.95%) were ordered from Goodfellow, Cambridge Ltd., U.K. Samples of 15-mm diameter and 2-mm thickness were cut from the foil and served as working electrodes. Samples were abraded with emery papers down to 4000 SiC, cleaned in an ultrasonic bath for 2 min and finally rinsed with distilled water. They were embedded in a Teflon holder to expose an area of 0.785 cm^2 to the solution. Carbon rod and a saturated calomel electrode (SCE) served as counter electrode and reference electrode, respectively, in a conventional three-electrode corrosion cell (PAR EG&G Model K0047). Potentials in the text refer to the SCE scale. A PAR EG&G Model 263 potentiostat/galvanostat controlled by M270 software was used for electrochemical measurements.

Measurements were performed in aerated borate buffer (0.002 M NaOH and 0.022 M $Na_2B_4O_7{\cdot}10\ H_20$), pH 9.2, prepared from p.a. chemicals and deionised water. The addition of NaCl was studied in a concentration range from 0.01 to 1 M (0.01, 0.0125, 0.02, 0.03, 0.04, 0.05, 0.1, 0.125, 0.2, 0.3, 0.5 and 1 M).

Cyclic voltammograms were recorded at a scan rate of 10 mVs^{-1}, unless stated otherwise. Prior to the chronopotentiometric experiment the potential was jumped from cathodic potential of −1.0 V to the anodic potential of interest, E_t, than the electrode was polarised by a constant current of 0.1 mA and the E_t–t decay curves were recorded for 300 s. After electrochemical measurements the electrode surface was checked routinely with an Olympus SZH 10 stereomicroscope.

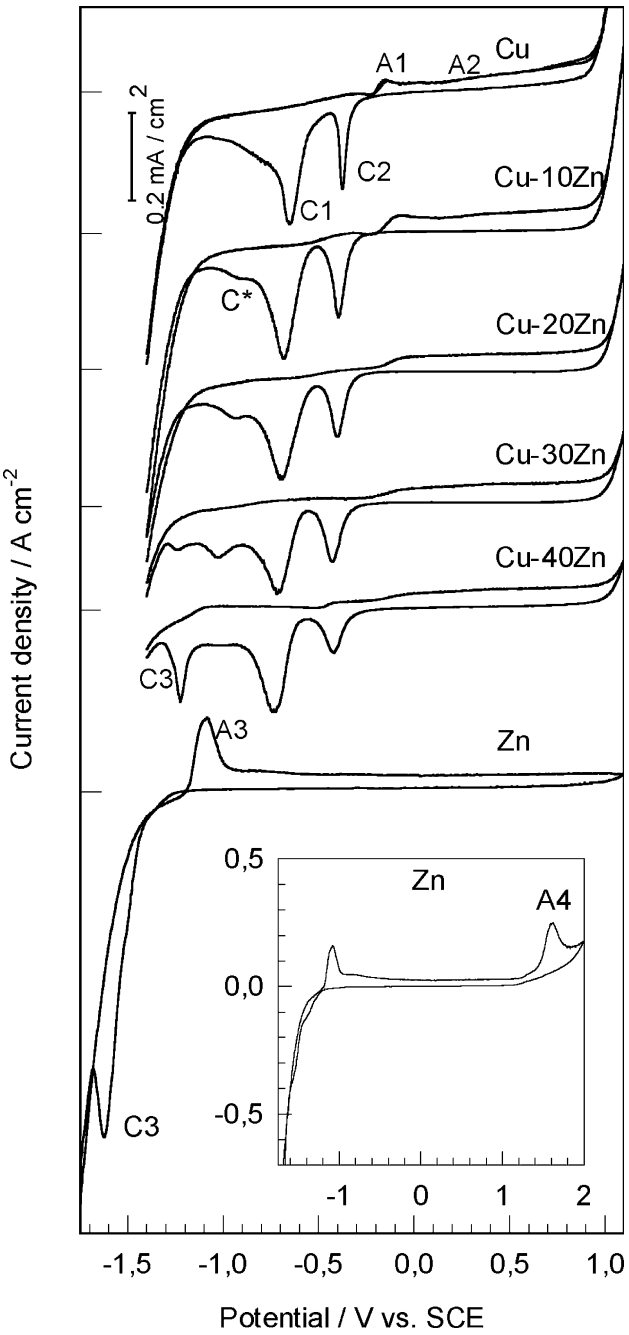

Fig. 1. Cyclic voltammograms of Cu, Cu–*x*Zn (*x* = 10–40 wt.%) and Zn in borate buffer, pH = 9.2, recorded at 10 mV s^{-1}. The inset shows the Zn voltammogram recorded up to 2.0 V.

3. Results

3.1. *Measurements in borate buffer (pH 9.2)*

Cyclic voltammograms recorded in borate buffer for Cu and Zn metals and four types of brasses (Cu–10Zn, Cu–20Zn, Cu–30Zn and Cu–40Zn) offer a good overview and enable a comparison of the current peaks and corresponding electrochemical processes taking place on the materials investigated (Figure 1). Cyclic voltammograms were recorded in the range from −1.4 V to 1.1 V for Cu and Cu–*x*Zn alloys, and from −1.75 to 1.1 V for Zn. Electrochemical reactions involved in the anodic and cathodic parts of the voltammetric response of copper have already been discussed [24–26]. The anodic peak A1 at −0.05 V (Figure 1) corresponds to the oxidation of Cu to Cu_2O according to the reaction:

$$2Cu + H_2O = Cu_2O + 2H^+ + 2e^- \quad (1)$$

The oxidation proceeds further through the broad passive region A2 according to the reaction:

$$Cu_2O + H_2O = 2CuO + 2H^+ + 2e^- \quad (2)$$

These reactions result in the formation of a duplex oxide layer with inner Cu_2O and outer hydrated CuO layers, the overall structure being denoted as $Cu/Cu_2O/CuO$ [24–26]. The passive range is limited by oxygen evolu-

tion at $E > 1.0$ V. In the cathodic scan the reduction proceeds in two steps. In the region of peak C2, the outer CuO is reduced to Cu_2O, which is then reduced to Cu in the region of peak C1. For the anodic potential limit $E_a < 0$ V, C1 is the only peak observed in the cathodic cycle. At more positive E_a, peak C2 appears.

Zinc metal exhibits an anodic peak A3 at a rather negative electrode potential of −1.1 V, which is in accordance with the equilibrium potential of −1.18 V vs. SCE [21] for the reaction at pH 9.2:

$$Zn + 2OH^- = ZnO + H_2O + 2e^-. \quad (3)$$

Following the peak A3, a broad passive region is established which extends up to 1.4 V. Here it is limited by trans-passive oxidation, denoted by the second anodic peak A4 at 1.6 V related to the formation of species of higher valence, Zn_2O_3, Zn_3O_5 or ZnO_2 (inset in Figure 1) [27]. A cathodic peak, C3, is observed for anodic potential limits more positive than −0.9 V. It shifts from −1.3 V to −1.6 V as E_a becomes more positive. For $E_a > 1.5$ V, peak C3 is no longer observed, as it becomes hidden by the hydrogen evolution curve.

The shape of the cyclic voltammograms recorded for the four different types of brass is, in general, more similar to that for Cu than for Zn metal. Voltammograms for Cu–10Zn and Cu–20Zn alloys are very similar to that for copper, except for a slight decrease in current density of the cathodic peaks C1 and C2. A small cathodic peak C* appears at −1.0 V, and is ascribed to the electrodeposition of soluble Cu(II) species [16, 30]. It increases with increasing time of polarization at $E > 0.9$ V, where the formation of soluble Cu(II) species is expected [16]. As the zinc content in the alloy increases, several features originating from zinc can be observed. The voltammogram of Cu–30Zn alloy contains a new peak C3 at −1.3 V in the cathodic cycle. This peak becomes more pronounced as the content of Zn is increased to 40 wt.%. This increase of peak C3 is related to the appearance of a new anodic peak A3. Moreover, for $E_a < 0.3$ V, peaks A3 and C3 are the only peaks in the cyclic voltammograms. Comparison with the voltammogram for Zn metal indicates that peaks A3 and C3 are related to the oxidation and reduction, respectively, of the ZnO layer. Due to the formation of this layer, the hydrogen evolution reaction for alloys with higher zinc contents is shifted by approximately 200 mV towards more negative potentials.

Cyclic voltammograms were recorded as a function of scan rate for Cu–10Zn and Cu–40Zn alloys within the potential limits of −1.4 V and 1.1 V (Figure 2). Anodic plateau A1 and two cathodic peaks C1 and C2 are observed for Cu–10Zn alloy, whereas for Cu–40Zn alloy, anodic peak A3 and anodic plateau A1, and cathodic peaks C1, C2 and C3 are observed. Anodic plateau A1 of Cu–40Zn alloy can be observed only for $\nu \geq 20$ mV s^{-1}. The current density of the anodic and cathodic peaks increases linearly with $\nu^{1/2}$ (Figure 3). The straight lines of anodic peak currents i_p vs. $\nu^{1/2}$ originate at the origin and have a slope of approximately 0.5 (0.51 for Cu–10Zn and 0.52 for Cu–40Zn) (Figure 3a) [31]. Peaks C1 and C2 of the Cu–10Zn alloy also show a linear dependence, with slopes of −3.1 and −1.8, respectively, whereas for Cu–40Zn alloy, the same peaks exhibit slopes of −2.3 and −1.1 (Figure 3b). Peak C3 gives a slope of −3.9. The potentials of the anodic peak and cathodic peaks move, with increasing scan rate, towards more positive and negative values, respectively. The dependence of peak potential E_p on log ν for peak A1 has slopes of 40 mV/decade and 45 mV/decade for Cu–10Zn and Cu–40Zn, respectively (Figure 3c). For cathodic peaks C1 and C2 of Cu–10Zn alloy the slopes of E_p vs. log ν are 110 and 95 mV/decade, respectively (Figure 3d). For Cu–40Zn alloys, peaks C1 and C2 give slopes of 90 and 62 mV/decade, whereas a value of 84 mV/decade was obtained for peak C3.

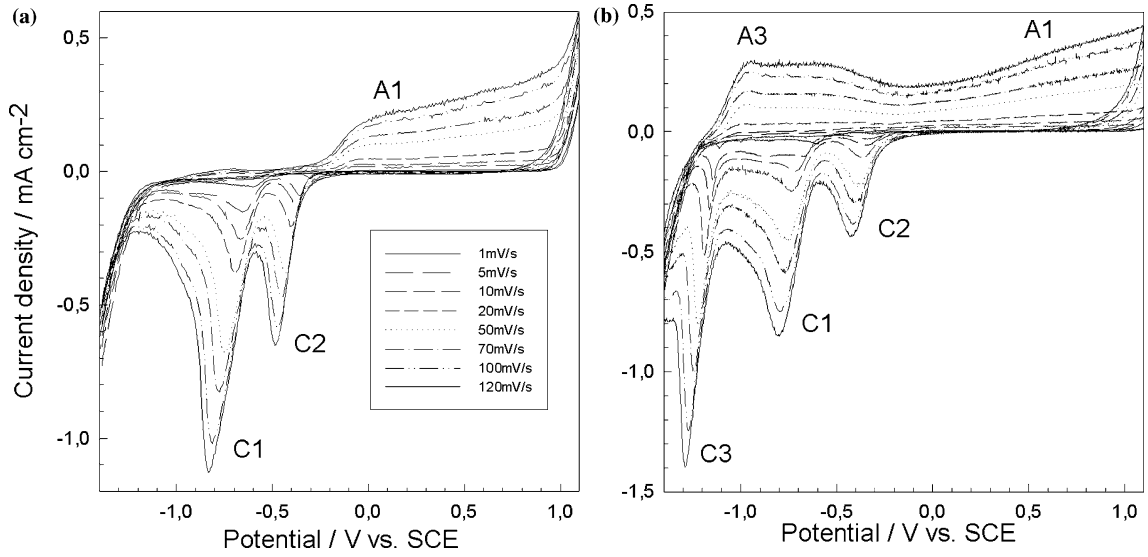

Fig. 2. Cyclic voltammograms of (a) Cu–10Zn and (b) Cu–40Zn recorded in borate buffer, pH = 9.2, at various potential scan rates.

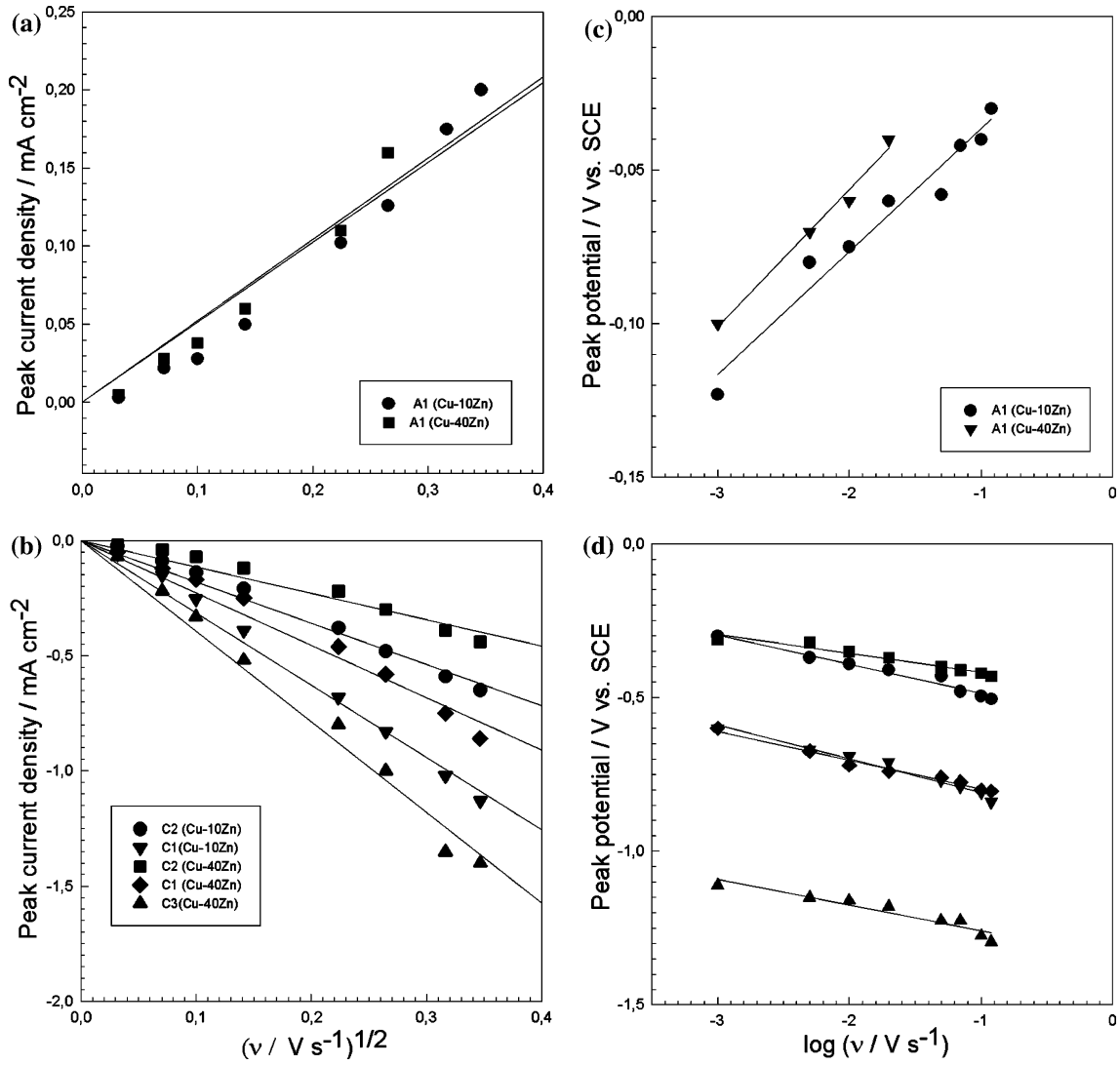

Fig. 3. Relationships i_p vs. $\nu^{1/2}$ and E vs. log ν for anodic peak A1 and cathodic peaks C1, C2 and C3 were determined from the cyclic voltammograms presented in Figure 2.

The process of electroreduction, observed in the chronopotentiometric $E-t$ decay curves and characterized by a potential plateau, was recorded after polarization to various electrode potentials, E_t. Its extent is denoted as the transient time, τ, which is, according to the Sand's equation [31, 32], related to the amount of reduced species at the electrode surface. Depending on the value of E_t, two or three potential plateaus appear in the decay curves (Figure 4). For $E_t \leqslant 0$ V the plateau was not well defined but, for $E_t \geqslant 0.1$ V, two or three well-defined plateaus appeared (Table 1, Figure 4). $E-t$ decay curves were recorded for Cu, Zn and the four Cu–xZn alloys at E_t values of 0.3 V and 0.7 V were shown in Figure 4. The related transient times, τ_1, τ_2 and τ_3, determined from $E-t$ curves according to the method of Laity–McIntyre [31, p. 317], are presented for E_t of 0.3 V, 0.5 V and 0.7 V (Table 1). For Cu metal, the plateaus at −0.2 V and −0.5 V are analogous to the current peaks in Figure 1 and correspond to the reduction of CuO and Cu_2O, respectively. Zinc shows only one plateau at −1.2 V, in accordance with the reduction of ZnO at peak C3 in Figure 1. From the measured transition times and the constant current of 0.1 mA used in the experiments, the charge density, Q, can be calculated, taking into account the electrode area and current efficiency of 100%. The values of charge density can then be used to calculate the layer thickness [16]. The thickness of the Cu_2O layer was calculated according to the relation $d_{Cu_2O} = (Q_{\tau 1} - Q_{\tau 2})\ V_{Cu_2O}/2r\mathrm{F}$, where the molar volume $V_{Cu_2O} = 23.9\ \mathrm{cm^3\ mol^{-1}}$, F is the Faraday constant, 96487 C $\mathrm{mol^{-1}}$, and Q is the calculated charge in C $\mathrm{cm^{-2}}$. The roughness factor r is assumed to be 1. The thickness of CuO was calculated according to the relation $d_{CuO} = Q_{\tau 2}\ V_{CuO}/r\mathrm{F}$, where $V_{CuO} = 12.4\ \mathrm{cm^3\ mol^{-1}}$. The thickness of ZnO was similarly calculated according to the relation $d_{ZnO} = Q_{\tau 3}\ V_{ZnO}/2r\mathrm{F}$, where $V_{ZnO} = 14.9\ \mathrm{cm^3\ mol^{-1}}$. The values of thickness are presented in Table 1.

The extent of plateaus τ_1 and τ_2 decreases from Cu–10Zn towards Cu–40Zn, with the calculated thickness of

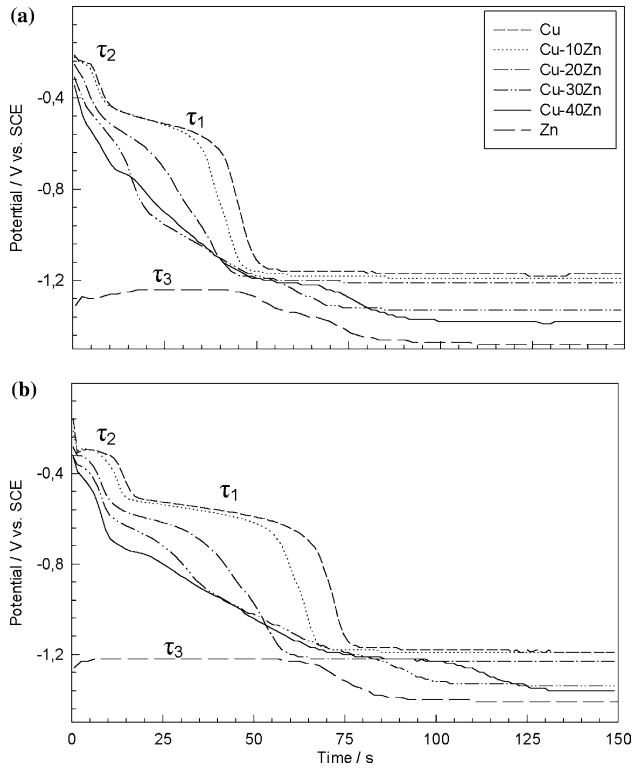

Fig. 4. Chronopotentiometric curves for Cu, Zn, and Cu–*x*Zn (x = 10–40 wt.%) were recorded at cathodic current 0.1 mA following the polarisation of the electrodes at the potentials of (a) 0.3 V and (b) 0.7 V for 1 min.

Table 1. Transient times, τ_1, τ_2 and τ_3, and calculated thickness, d_1,d_2 and d_3, of passive layers for plateaus C1, C2 and C3 for Cu, Cu–*x*Zn (x = 10–40%) and Zn, recorded at potential limits, E_t, at a constant current of 0.1 mA

	τ_1/s	d_1/nm	τ_2/s	d_2/nm	τ_3/s	d_3/nm
E_t = 0.3 V						
Cu	30	3.8	6	0.98		
Cu–10Zn	28	3.6	5	0.82		
Cu–20Zn	20	3.2	Undefined			
Cu–30Zn	7	1.1	Undefined		20	2.0
Cu–40Zn	5	0.8	Undefined		26	2.6
Zn					31	3.0
E_t = 0.5 V						
Cu	41	5.0	9	1.5		
Cu–10Zn	29	3.4	7.5	1.2		
Cu–20Zn	21	2.7	4	0.66		
Cu–30Zn	12	1.4	3	0.49	21	2.1
Cu–40Zn	8	0.79	3	0.49	35	3.4
Zn					52	5.1
E_t = 0.7 V						
Cu	49	6.0	11	1.9		
Cu–10Zn	41	5.0	9	1.5		
Cu–20Zn	29	3.6	6	0.98		
Cu–30Zn	19	2.2	5	0.82	17	1.7
Cu–40Zn	15	1.7	4	0.65	40	3.9
Zn					62	6.1

Cu_2O decreasing from 5.0 nm for Cu–10Zn to 1.7 nm for Cu–40Zn alloy at E_t = 0.7 V, and that of CuO decreasing from 1.5 to 0.65 nm (Table 1). For Cu–30Zn and Cu–40Zn alloys a new plateau τ_3 appears at −1.2 V which, by comparison with the curve for Zn, corresponds to the reduction of ZnO. The calculated thickness of ZnO is greater for Cu–40Zn (3.9 nm) than for Cu–30Zn alloy (1.7 nm) at E_t = 0.5 V (Table 1). The thickness of Cu_2O and CuO oxide layers formed on Cu–*x*Zn alloys is smaller than that formed on Cu metal. Similarly, the thickness of the ZnO oxide formed on Cu–*x*Zn alloys is smaller than that on Zn metal. It should be noted, however, that the calculation of thickness is subject to certain limitations, since the passive layer has been shown probably to be composed of mixed copper and zinc oxides and not of structured oxide layers [16].

The chronopotentiometric experiments show that the formation of ZnO not only diminishes the formation of copper oxides, as indicated by a decrease in thickness, but also substantially delays the formation of CuO. The latter finding is supported by the fact that the potential limit E_t, after which the corresponding plateau τ_2 appears in E–t decay curves, is shifted to more negative potentials. In the case of Cu and Cu–10Zn plateaus, τ_2 appears at $E_t \geq 0.3$ V but, for alloys with higher zinc content, only at $E_t \geq 0.5$ V (Figure 4).

3.2. *Measurements in borate buffer containing chloride ions*

The addition of chloride ions to borate buffer induces localized pitting corrosion of the materials investigated. This process exhibits several typical features in cyclic voltammograms – narrowing of the passive region due to a sudden increase in current density at the breakdown potential E_b, a current hysteresis loop following the scan reversal, and increase in charge of the cathodic peaks. This behaviour is illustrated in Figure 5 for Cu, Cu–10Zn, Cu–40Zn and Zn in the presence of four different NaCl concentrations. The values of E_b shift towards more negative values as the NaCl concentration is increased. The charge associated with cathodic peak C2 increases significantly due to the increased formation of corrosion products in the course of the breakdown process. Cu–10Zn alloy shows slightly more negative values of E_b than for Cu, whereas Cu–40Zn alloy shows significantly more negative values than for both Cu and Cu–10Zn. In general, the value of E_b shifts towards more negative potentials at higher zinc content, as discussed in detail below. The values of E_b for Cu–40Zn alloy show a much narrower span with increasing NaCl concentration than those for Cu and Cu–10Zn alloy. This behaviour is similar to zinc metal (Figure 5d). It is noteworthy that the height of peak C3 for zinc is not significantly affected by NaCl concentration, indicating that the majority of species formed in chloride containing media are dissolved.

Several ways of determining the value of E_b have been used [18, 34, 35]. From cyclic voltammograms recorded at 0.2 mV s^{-1}, it has been defined as the highest positive potential involving an anodic current in the passive

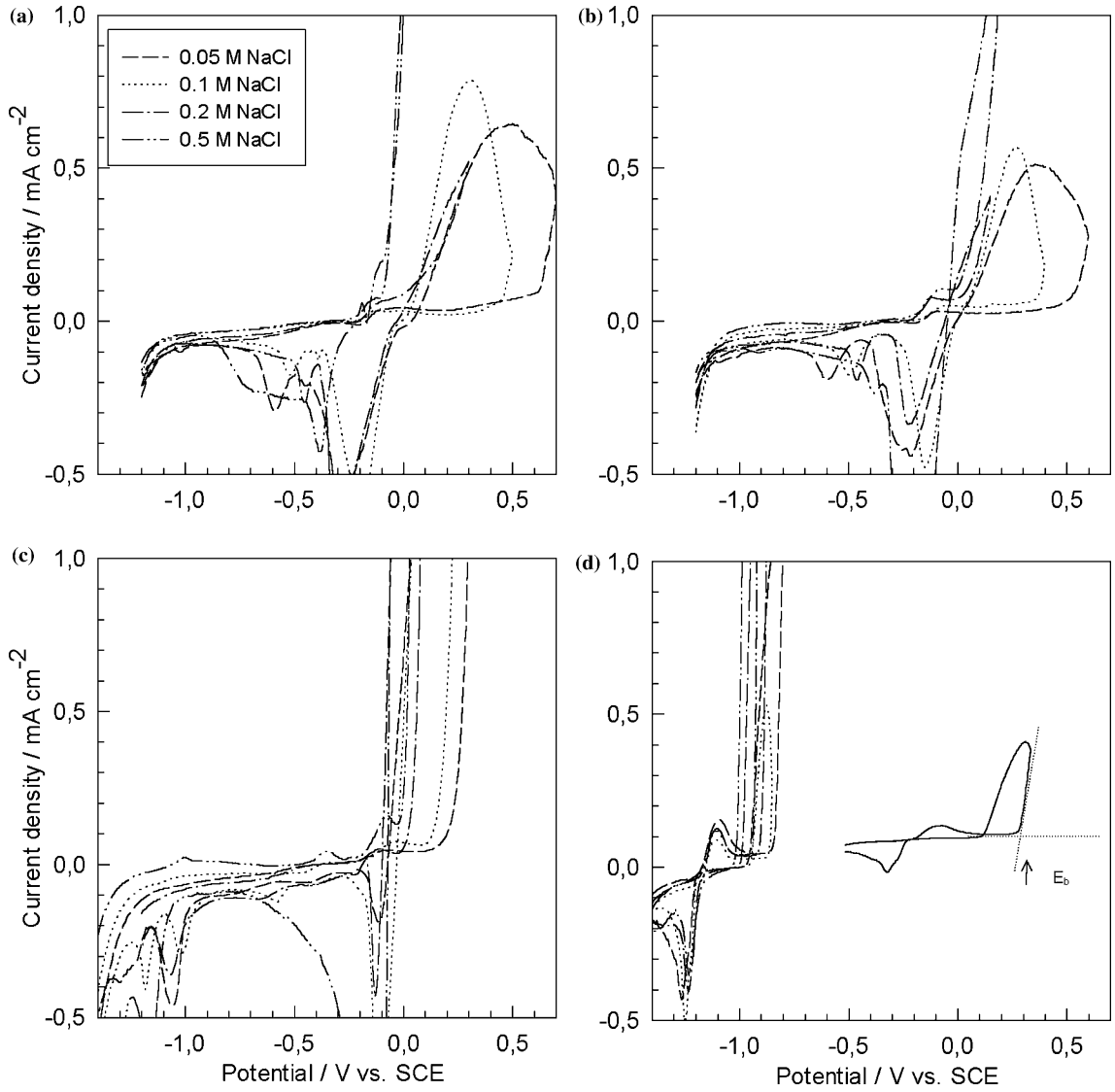

Fig. 5. Cyclic voltammograms recorded for (a) Cu, (b) Cu–10Zn, (c) Cu–40Zn and (d) Zn in borate buffer, pH = 9.2, containing 0.05 M, 0.1 M, 0.2 M and 0.5 M NaCl. The inset in (d) presents the determination of the breakdown potential, E_b, $\nu = 10$ mV s^{-1}.

range [17]. From anodic polarization curves recorded at 0.3 mV s^{-1}, it has been defined as the potential at which the current density reaches the value of 0.1 mA cm^{-2} [34]. Yet another way to determine E_b was from E_b vs. ν plots, by extrapolating to zero potential scan rate [35]. In the present work the breakdown potential was determined from cyclic voltammograms as the intercept of the tangents drawn at the point of sudden current density increase in the passive region (inset in Figure 5d). E_b was determined in the presence of 12 NaCl concentrations ranging from 0.01 M to 1.0 M for Cu and Zn metals and the four Cu–xZn alloys (Figure 6). Generally, a common relationship between E_b and NaCl concentration according to equation $E_b = a + b \log c_{NaCl}$ is established, with straight lines drawn in a way to obtain a minimal relative error by least square method (Table 2). For Cu metal, E_b obeys the above logarithmic relation over the whole concentration range studied, with the constant $b = -0.28$ V/decade c_{NaCl}. Zinc is susceptible to pitting corrosion already at low chloride concentrations and increasing concentration does not shift E_b significantly towards more negative potentials, i.e., the slope is small ($b = -0.05$ V/decade c_{NaCl}). The relationships for the four Cu–xZn alloys lie between these two limiting cases. A critical concentration, c_{crit}, exists at which a change in the slope occurs. The value of c_{crit} is dependent on the zinc content in the alloy and decreases linearly from 0.14 M for Cu–10Zn to 0.04 M for Cu–40Zn (Table 2). For $c < c_{crit}$ the slope for Cu–10Zn alloy is −0.34 V/decade c_{NaCl}, similar to that for Cu (−0.28 V/decade c_{NaCl}). The slope increases with increasing zinc content to −0.51 V/decade c_{NaCl} for Cu–40Zn alloy. For $c > c_{crit}$, lower slopes are obtained, from −0.11 to −0.06 V/decade c_{NaCl}, thus more similar to that for Zn (−0.05 V/decade c_{NaCl}). These results indicate that, for $c < c_{crit}$, Cu–10Zn alloy is the most resistant towards localized pitting corrosion. Resistance decreases with increasing zinc content to 40 wt.%. As the c_{crit} for Cu–10Zn is exceeded, the difference between particular alloys

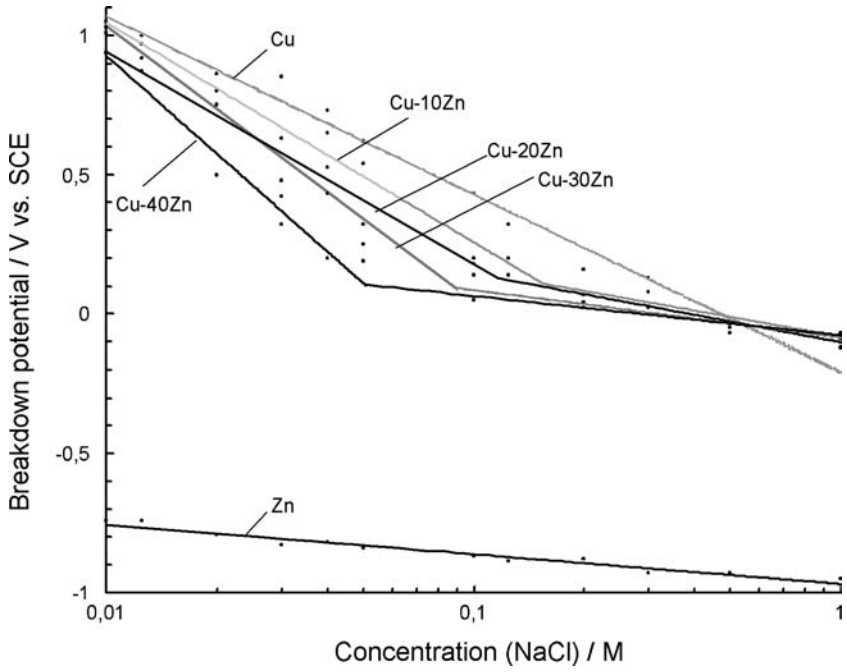

Fig. 6. Relationship between E_b and logarithm of chloride concentration for Cu, Zn and four Cu–xZn alloys (x = 10, 20, 30 and 40 wt.%).

Table 2. General relationship $E_b = a + b \log c_{NaCl}$ determined from voltammetric curves

Material	$C_{NaCl} < C_{crit.}$	R^2	$C_{crit.}$/M	$C_{NaCl} > C_{crit.}$	R^2
Cu	$E_b = -0.21 - 0.28 \log c$	0.98			
Cu–10Zn	$E_b = -0.53 - 0.34 \log c$	0.98	0.14	$E_b = -0.08 - 0.10 \log c$	0.82
Cu–20Zn	$E_b = -0.59 - 0.33 \log c$	0.96	0.125	$E_b = -0.10 - 0.11 \log c$	0.95
Cu–30Zn	$E_b = -0.95 - 0.43 \log c$	0.93	0.09	$E_b = -0.09 - 0.08 \log c$	0.92
Cu–40Zn	$E_b = -1.40 - 0.51 \log c$	0.97	0.04	$E_b = -0.07 - 0.06 \log c$	0.83
Zn	$E_b = -0.97 - 0.05 \log c$	0.95			

becomes smaller and, for $c_{NaCl} > 0.14$ M, all four alloys show similar values of E_b, with Cu–10Zn alloy still being the most resistant.

The electrode surface was examined for changes accompanying the above phenomena. Potentiodynamic scans were interrupted at a potential slightly above E_b and the potential was then held at constant value for 2 min. Following this, an image of the surface was taken with a stereomicroscope. Cu and Zn metals and Cu–10Zn and Cu–40Zn alloys were investigated in borate buffer containing NaCl concentrations of 0.05 M, 0.1 M, 0.2 M and 0.5 M (Figure 7). The corresponding constant potentials were 0.6, 0.4, 0.2 and 0.1 V. Insets in Figure 7 show the resulting images of the electrode surface. Cu and Cu–10Zn alloy show similar behaviour in the presence of 0.05 M NaCl, with the beginning of passive film breakdown at 0.61 and 0.55 V (Figure 7a). Spots of blue–green corrosion product, presumably the oxychloride $CuCl_2 \cdot 3CuO \cdot 4H_2O$, were observed on the surface of Cu–10Zn alloy covered with a red layer of Cu_2O. Copper suffers almost no apparent corrosion, including the formation of oxychloride. E_b of Cu–40Zn alloy is more negative by 200 mV than that for Cu or Cu–10Zn, and is accompanied by a sharp increase in current density and the formation of large amounts of blue–green oxychloride. At higher concentrations of NaCl, the E_b values for Cu–40Zn remained always more negative than those for Cu and Cu–10Zn (Figure 7b–d). Zinc metal is very susceptible to localized corrosion. As discussed above, its passive region almost disappears with the addition of only a small amount of chloride ions. In the presence of only 0.05 M NaCl the E_b value shifts to −0.75 V, as compared to chloride-free borate buffer, where the passive region extends to 1.4 V (Figure 1). A large increase in current density leads to pitting corrosion. Localized corrosion is accompanied, in the course of potentiostatic oxidation, by the formation of small spots of whitish corrosion products, which correspond to ZnO and/or $ZnCl_2$. At higher chloride concentrations, the localized corrosion progresses with numerous deep small pits and a large amount of voluminous whitish corrosion product, which accumulates at the bottom of the cell.

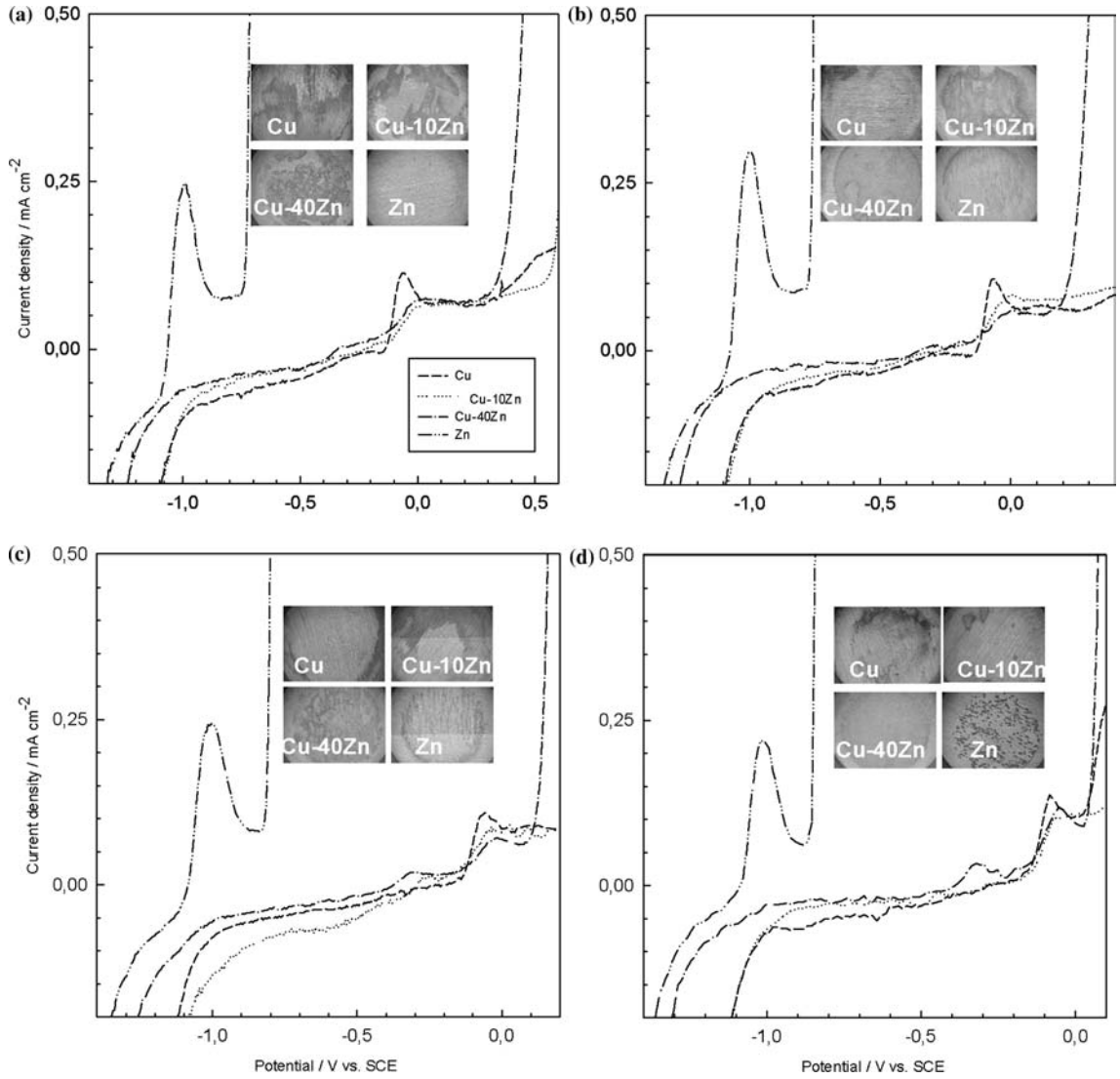

Fig. 7. The anodic part of cyclic voltammograms recorded for Cu, Cu–10Zn, Cu–40Zn and Zn in borate buffer containing (a) 0.05 M, (b) 0.1 M, (c) 0.2 M and (d) 0.5 M NaCl. Scan rate was 10 mV s^{-1}. Photo insets are microscope images (magnification 7×) of the electrode surface after potentiostatic polarization at 0.6 V, 0.4 V, 0.2 V and 0.1 V for 2 min.

4. Discussion

The electrochemical characteristics of a series of Cu–*x*Zn alloys and their comparison with those of the individual metal components show that the passivation in borate buffer of alloys with $x \leqslant 30$ wt.% is governed mainly by the copper component. This is in agreement with observations on other copper alloys, such as Cu–Ni alloys [33, 34, 36] and Cu–Ag [37], where the passivation of alloys with high copper content resulted in the formation of Cu oxide-rich passive film. The thickness of the Cu-oxide layer decreases and that of Zn-oxide increases with increasing zinc content (Table 1, Figure 4). In keeping with this, Morales et al. showed that the outer region of the passive film on α-brass (71Cu–28Zn) is richer in Cu_2O than on β-brass (52Cu–47Zn) [19]. Even though electrochemical characteristics of Cu–10Zn alloy do not indicate the presence of ZnO in the oxide film, XPS spectra have shown the formation of a thin Zn oxide layer at potentials close to those at which Cu_2O forms [16].

The increased formation of ZnO progressively delays the formation of Cu-oxides in alloys with higher zinc contents, as shown by the chronopotentiometric experiments (Figure 4), as well as by XPS analysis [16]. Kim et al. also emphasized that the formation of ZnO suppressed the subsequent copper oxidation [15]. The oxidation potential of Zn in brass was more positive than that of pure zinc, which may result from the alloying effect between copper and zinc in the brass solid solution [15]. Based on these findings, it is clear that the addition of zinc to the bulk material of copper changes not only the physical, electrical and mechanical properties, but also the structure and properties of its passive film. The investigation of the structure of the passive film by angle resolved XPS measurements yielded no clear conclusion regarding the layer structure [16]. It was therefore assumed that the passive

layer is not structured but is rather a mixed oxide layer whose composition and/or structure may change with depth [16].

The experimentally determined E_b vs. log c_{NaCl} straight lines for Cu and Zn are well separate from each other (Figure 6). Straight lines for Cu–xZn alloys are closer to that for Cu metal but always more negative. Our previous study on Cu–xNi alloys has shown that E_b vs. log c_{NaCl} straight lines for Cu and Ni metals have a cross-section [38]. Consequently, at lower chloride concentrations, an increase in nickel content reduced the resistance to pitting corrosion whereas, at higher chloride concentrations, an increase in nickel content was beneficial. In the case of Cu–xZn alloys, an increase in zinc content is detrimental regardless of the chloride concentration range. Therefore, ZnO/Cu_2O/CuO-structured passive film is less resistant to pitting corrosion than the Cu_2O/CuO structure formed on Cu metal, however, significantly more resistant than ZnO formed on Zn metal. Similar results were observed by Morales et al. for α-, (α + β)- and β-brasses with Zn contents of 28, 39 and 48 wt.%, respectively [17]. With increasing zinc content in the alloy the resistance towards localized corrosion in the presence of 0.01–0.5 M NaCl decreased [18]. The improvement of localized corrosion resistance is especially significant in the lower potential range, i.e., where zinc itself is active. In this range only the dissolution of zinc, with formation of ZnO, is expected for Zn metal, as well as for Cu–xZn alloys, since the oxidation of copper becomes feasible only at more positive potentials, i.e. $E^{\emptyset}_{Zn^{2+}/Zn} = -0.76$ V SHE and $E^{\emptyset}_{Cu^{2+}/Cu} = 0.34$ V SHE [21]. Therefore, despite the fact that ZnO layer is formed on Zn metal and Cu–xZn alloys, the latter is significantly more corrosion resistant. Morales et al. suggested that selective Zn dissolution in the lower potential range leaves the underlying surface enriched in copper [17]. Our previous study, where the dissolution of Cu and Zn metals and Cu–xZn alloys were investigated by differential anodic pulse stripping (DAPS) voltammetry [23], corroborates such as explanation. During polarization at potentials preceding the anodic peak A1, only zinc ions were detected in the solution, indicating the exclusive dissolution of zinc [23]. The measured concentration of dissolved zinc was almost two orders of magnitude higher for Cu–40Zn than for Cu–10Zn alloy. At potentials more positive than the anodic peak both zinc and copper ions were detected in solution, indicating that simultaneous dissolution of both components takes place. Their ratio in the solution was not the same as that in the bulk alloy, since the concentration of dissolved zinc was much higher than that of dissolved copper.

Therefore, the Cu-rich sub-layer/ZnO/Cu_2O/CuO is more resistant to pitting corrosion than the ZnO layer formed on Zn metal, since the Cu-rich sub-layer at the alloy/film interface is resistant to corrosion at negative potentials where Zn metal is otherwise susceptible to pitting corrosion. On the other hand, such a structure is less resistant than the Cu_2O/CuO passive film formed on Cu metal. This indicates that the incorporation of ZnO in the passive film is not beneficial and promotes corrosion. El- Sherif et al. showed that E_b values shifted in a more negative direction with increasing zinc content (5.5–38 wt.%), whereas a shift towards more positive values was observed with increasing lead content [39]. The increasing current density with increasing zinc content in 0.6 M NaCl was ascribed to the preferential dissolution of zinc, which increased the disproportionation and/or displacement reaction leading to the redeposition of Cu. The latter process increases the cathodic area distribution, causing the formation of active galvanic couples, and increases the corrosion rate of Cu–Zn alloys [39]. Such an explanation supports the results presented in this work, since the incorporation of ZnO in the Cu_2O/CuO-structured passive film proved to have a negative effect on corrosion resistance in chloride containing solution.

5. Conclusions

Electrochemical methods of cyclic voltammetry and chronopotentiometry were used to study the formation and composition of the passive film formed on four Cu–xZn (x = 10–40 wt.%) alloys. Individual metal components were studied for a thorough comparison. The general properties of Cu–xZn alloys resemble those of copper more than those of zinc. With increasing zinc content the formation of ZnO also increases, thus delaying and diminishing the formation of Cu oxides.

The addition of chloride ions to borate buffer alters substantially the behaviour of the alloys and their constituent metals. Over a wide range of chloride concentrations, Cu, followed by Cu–10Zn alloy, is the most resistant to pitting corrosion, whereas Cu–40Zn alloy is the least resistant. Zinc is susceptible to pitting corrosion, even at low chloride concentrations, and shows the least resistance of all the materials investigated. Values of breakdown potentials, E_b, are dependent on chloride concentration and zinc content. E_b for Cu–xZn alloys decrease with increasing NaCl concentration up to a certain critical concentration, $c_{crit.}$, after which further increase of NaCl does not significantly affect E_b, and the difference between alloys becomes insignificant.

The structure of the passive film changes from Cu_2O/CuO, through ZnO/Cu_2O/CuO, to ZnO. The resistance of Cu–xZn alloys is poorer than that of copper metal, but significantly better than for zinc metal. The results are interpreted in terms of the advantageous formation of a Cu-rich sublayer which is resistant to corrosion at negative potentials, at which zinc metal is otherwise susceptible to localized corrosion.

Acknowledgements

The authors acknowledge financial support from the Slovenian Research Agency through grant No. P2-0148. Copper-zinc specimens were donated by Wieland-Werke AG, Ulm, Germany.

References

1. A.P. Pchelnikov, A.D. Sitnikov, I.K. Marshakov and V.V. Losev, *Electrochim. Acta* **26** (1981) 591.
2. A.V. Polunin, A.P. Pchelnikov, V.V. Losev and I.K. Marshakov, *Electrochim. Acta* **27** (1982) 467.
3. R.K. Dinnappa and S.M. Mayanna, *Corros. Sci.* **27** (1987) 349.
4. S.H. Sanad, H. Abbas, A.A. Ismail and K.M. El-Sobki, *Surf. Technol.* **25** (1985) 39.
5. H.C. Shih and R.J. Tzou, *J. Electrochim. Soc.* **138** (1991) 958.
6. V. Otieno-Alego, G.A. Hope, T. Notoya and D.P. Schweinsberg, *Corros. Sci.* **38** (1996) 213.
7. A.M. Fenelon and C.B. Breslin, *J. Appl. Electrochem.* **31** (2001) 509.
8. M.M. Osman, *Mater. Chem. Psys.* **71** (2001) 12.
9. A. Nagiub and F. Mansfeld, *Corros. Sci.* **43** (2001) 2147.
10. A.T. Cole, R.C. Newman and K. Sieradzki, *Corros. Sci.* **28** (1988) 109.
11. T. Shahrabi, R.C. Newman and K. Sieradzki, *J. Electrochim. Soc.* **140** (1993) 348.
12. V.A. Kolotyrkin, V.N. Chervyakov, A.P. Pschelnikov and V.V. Losev, *Prot. Met.* **31** (1995) 220.
13. D. Tromans, *Corros. Sci.* **39** (1997) 1307.
14. X. Guo, K. Gao, L. Qiao and W. Chu, *Metal Mater. Trans. A* **32A** (2001) 309.
15. B.S. Kim, T. Piao, S.N. Hoier and S.M. Park, *Corros. Sci.* **37** (1995) 557.
16. I. Milošev and H.-H. Strehblow, *J. Electrochem. Soc.* **150** (2003) 517.
17. J. Morales, G.T. Fernandez, P. Esparza, S. Gonzalez, R.C. Salvarezza and A.J. Arvia, *Corros. Sci.* **37** (1995) 211.
18. J. Morales, G.T. Fernandez, P. Esparza, S. Gonzalez, R.C. Salvarezza and A.J. Arvia, *Corros. Sci.* **40** (1998) 177.
19. J. Morales, P. Esparza, G.T. Fernandez, S. Gonzalez, J.E. Garcia, J. Caceres, R.C. Salvarezza and A.J. Arvia, *Corros. Sci.* **37** (1995) 231.
20. A.L. Rudd and C.B. Breslin, *Electrochim. Acta* **45** (2000) 4015.
21. M. Pourbaix, *Atlas of Electrochemical Equilibria in Aqueous solutions* (NACE, Cebelcor, Houston, Brussels, 1974).
22. F.M. Al-Kharafi, B.G. Ateya and R.M. Abd Allah, *J. Appl. Electrochem.* **34** (2004) 47.
23. I. Milošev and A. Minović, *Annali di Chimica* **91** (2001) 343.
24. H.-H. Strehblow and H.-D. Speckman, *Werkst. Korros.* **35** (1984) 512.
25. J. Gomez Becerra, R.C. Salvarezza and A.J. Arvia, *Electrochim. Acta* **33** (1988) 613.
26. H-H. Strehblow, V. Maurice and P. Marcus, *Electrochim. Acta* **46** (2001) 3755.
27. D.D. Macdonald, K.M. Ismail and E. Sikora, *J. Electrochem. Soc.* **145** (1998) 3141.
28. H. Mishima, Mishima Lopez de, E. Santos, C.P. De Pauli, K. Azumi and N. Sato, *Electrochim. Acta* **36** (1991) 1491.
29. A.L. Rudd and C.B. Breslin, *J. Electrochem. Soc.* **147** (2000) 1401.
30. M.R. Gennero de Chialvo, S.L. Marchiano and A.J. Arvia, *J. Appl. Electrochem.* **14** (1984) 165.
31. I. Filipović and P. Sabioncello, Laboratorijski priručnik, Zagreb, 1978.
32. J. O'M Bockris and A.K.N. Reddy, 'Modern Electrochemistry', Vol. 2B, Electrodics in Chemistry, Engineering, Biology, and Environmental Science (Kluwer Academic/Plenum Publishers, New York, 2000).
33. M. Metikoš-Huković and I. Milošev, *J. Appl. Electrochem.* **22** (1992) 448.
34. I. Milošev and M. Metikoš-Huković, *J. Appl. Electrochem.* **29** (1999) 393.
35. I. Milošev, M. Metikoš-Huković, M. Drogowska, H. Menard and L. Brossard, *J. Electrochem. Soc.* **139** (1992) 2409.
36. P. Druska and H-H. Strehblow, *Surf. Inter. Anal.* **23** (1995) 440.
37. F.H. Assaf, A.M. Zaky and S.S. abd El-Rehim, *Appl. Surf. Sci.* **178** (2002) 18.
38. I. Milošev and M. Metikoš-Huković, *Electrochim. Acta* **42** (1997) 1537.
39. R.M. El-Sherif, K.M. Ismail and W.A. Badawy, *Electrochim. Acta* **49** (2004) 5139.